

Analyzing the Effects of MBPSS on the Transit Stability and High-Level Integration of Wind Farms during Fault Conditions

Bilel Dhouib

CEM Laboratory, Engineering School of Sfax, Tunisia
bilel.dhouib@enis.tn (corresponding author)

Mohamed Ali Zdiri

CEM Laboratory, Engineering School of Sfax, Tunisia
mohamed-ali.zdiri@enis.tn

Zuhair Alaas

Department of Electrical Engineering, Faculty of Engineering, Jazan University, Saudi Arabia
zalaas@jazanu.edu.sa

Hsan Hadj Abdallah

CEM Laboratory, Engineering School of Sfax, Tunisia
hsan.hajabdallah@enis.tn

Received: 7 March 2023 | Revised: 19 March 2023 | Accepted: 22 March 2023

Licensed under a CC-BY 4.0 license | Copyright (c) by the authors | DOI: <https://doi.org/10.48084/etasr.5838>

ABSTRACT

As the demand for renewable energy continues to increase, wind power has emerged as a prominent source of clean energy. However, incorporating wind energy into the power generation system at a high level can significantly impact the dynamic performance of the power system, resulting in increased uncertainties during operation. This study investigated the effectiveness of the Multi-Band Power System Stabilizer (MBPSS), a new power system stabilizer, in suppressing dynamic oscillations in a multi-machine power system connected to a wind farm. This research focused on analyzing the transient stability of a nine-bus network, commonly known as the Western System Coordinating Council (WSCC), integrated with a Doubly Fed Induction Generator (DFIG) using MATLAB/Simulink. The study evaluated the dynamic performance of the proposed system under fault conditions, including Line-to-Line-to-Line-to-Ground (LLLG) faults. Simulation results showed that MBPSS effectively dampened oscillations and improved the stability of the power system, even in the presence of severe faults and high-level integration of wind farms.

Keywords-wind farm; DFIG; MBPSS; LLLG fault; multimachine power system; transit stability

I. INTRODUCTION

Wind is a highly promising source of renewable energy, thanks to its environmental-friendly characteristics and widespread availability [1]. However, the current rate of integration of wind energy into the electricity grid remains relatively low. The large-scale integration of wind power sources presents potential technical challenges due to their intermittent nature, which must be carefully examined and addressed as part of the development of a sustainable energy system for the future [2-4].

The 9-bus system has been extensively used in power system analyses. In [5], a probabilistic load flow analysis was presented for the 9-bus WSCC system, using a stochastic

approach to validate the effectiveness of probabilistic analysis techniques to gain a more comprehensive understanding of power systems compared to deterministic analysis. The transient stability analysis of the IEEE-9 bus system under multiple contingencies was investigated in [6]. This study compared and employed both the Euler and Runge methods to examine changes in the frequency and rotor angle of the system under various fault conditions. The simulation results showed that the Runge method had a faster response. In [7], transient stability analysis was conducted on the IEEE 9-bus system, taking into account the integration of DFIG- and SCIG-based wind turbines. The simulation results showed that the DFIG-based wind turbine had a lower peak value of relative power angle than the SCIG-based one, but the results for settling time

were reversed. In [8], the transient stability assessment of an IEEE 9-Bus system integrated with a wind farm was investigated to evaluate its stability with DFIG integration.

Two techniques are used to improve oscillation damping and ensure system stability: Power System Stabilizers (PSSs) and FACTS systems have effects extensively documented [9-11]. However, while PSS is effective in damping local modes, it may not sufficiently address inter-zonal modes. Hence, various design approaches have been proposed to enhance PSS efficiency in damping diverse oscillation modes, such as the optimization of performance criteria to achieve optimal control [12], the use of neural networks in smart stabilizers [13], robust control [14], and fuzzy logic [15]. In summary, these controllers have been proven effective in addressing stability issues. This motivates the proposal of a novel power system stabilizer that integrates wind power generation for multi-machine systems. The implementation of MBPSS can significantly improve the primary frequency response of a power system. This is exemplified by the use of MBPSS at Hydro-Quebec (HQ) for several years [16]. Several studies, such as [17-19], highlighted the favorable effects of certain techniques on power systems. These techniques were shown to improve frequency response, global and electromechanical mode damping, and voltage stability. The improvements in the HQ transmission system can be attributed, at least in part, to its unique characteristics. HQ is isolated from the rest of the Eastern Interconnection and is characterized by a long radial structure, with power flow patterns established predominantly in the north-to-south direction.

This study investigated the integration of a wind farm that utilized DFIG as variable speed generators directly connected to the grid into a 9-bus network at a high level. The primary objective was to analyze the impact of wind farm integration on the transient stability of the power system, focusing on evaluating the effects of the MBPSS stabilizer. The evaluation of the system's transient state was based on analyzing the power angles, angular speeds, and frequencies of the synchronous generators. Additionally, fault scenarios, such as the LLLG fault, were considered to assess the system's dynamic performance. The main contributions of the current paper are:

- This study explored the effectiveness of an MBPSS that featured a three-frequency band structure (i.e. low-, intermediate-, and high-frequencies) for analyzing the system's transient stability.
- High-level integration of the wind farm was taken into account to improve the robustness of the MBPSS.
- The suggested system was exposed to high-level perturbation scenarios, including the LLLG fault, and the robustness of the controller was demonstrated to facilitate swift system recovery from these faults.

II. WIND FARM MODEL

A. Wind Speed Model

Accurate modeling of wind turbines is highly dependent on the wind speed model. While wind is often viewed as a random

phenomenon, its variability can be modeled using various approaches [20]. One way to represent the wind speed is to decompose it into a sum of harmonics, as demonstrated by [21]:

$$V_p(t) = 10 + 0.55[\sin(0.0393t) - 0.875 \sin(0.1178t) + 0.75 \sin(0.1963t) - 0.625 \sin(0.3927t) + 0.5 \sin(1.178t) + 0.25 \sin(1.9634t) + 0.125 \sin(3.9269t)] \quad (1)$$

B. Wind Turbine Model

A wind turbine aims to utilize wind energy and convert it into torque that rotates the rotor blades. The amount of wind energy converted into mechanical energy by the rotor is determined by three factors: density of the air, swept area of the rotor, and wind speed. Air density and wind speed are unique to each location and are considered climatic parameters [22]. The mathematical expression for the mechanical power output of a wind turbine is given by [23]:

$$P_m = C_p(\lambda, \beta) \frac{\rho A}{2} V_\omega^3 \quad (2)$$

The mechanical power harvested by the wind turbine and transferred to the rotor is represented by P_m (W). The turbine power coefficient is denoted by C_p , while ρ (kg/m^3) represents the density of the air, A (m^2) indicates the area swept by the rotor, V_ω (m/s) represents the wind speed, λ stands for the speed ratio, and β ($^\circ$) is the blade angle of inclination. Each wind turbine has its distinct power coefficient characteristics. As an example, the power coefficient for a 1.5MW wind turbine can be estimated through measurements and be approximated using [24]:

$$C_p(\lambda, \beta) = 0.5176 \left(\frac{116}{\lambda_i} - 0.4\beta - 5 \right) e^{-21/\lambda_i} + 0.0068 \lambda \quad (3)$$

The value of the λ_i parameter is determined by:

$$\frac{1}{\lambda_i} = \frac{1}{\lambda + 0.08\beta} - \frac{0.035}{\beta^3 + 1} \quad (4)$$

C. DFIG Model

The utilization of dynamic modeling for the DFIG in the rotating d - q reference frame yields the following equations [23-25]:

$$\begin{cases} v_{ds} = R_s i_{ds} - \omega_s \psi_{qs} + \frac{d\psi_{ds}}{dt} \\ v_{qs} = R_s i_{qs} + \omega_s \psi_{ds} + \frac{d\psi_{qs}}{dt} \\ v_{dr} = R_r i_{dr} - (\omega_s - \omega_r) \psi_{qr} + \frac{d\psi_{dr}}{dt} \\ v_{qr} = R_r i_{qr} + (\omega_s - \omega_r) \psi_{dr} + \frac{d\psi_{qr}}{dt} \end{cases} \quad (5)$$

where:

$$\begin{cases} \psi_{ds} = L_s i_{ds} + L_m i_{dr} \\ \psi_{qs} = L_s i_{qs} + L_m i_{qr} \\ \psi_{dr} = L_r i_{dr} + L_m i_{ds} \\ \psi_{qr} = L_r i_{qr} + L_m i_{qs} \end{cases}$$

The variables u_{ds} , u_{qs} , u_{dr} , and u_{qr} denote the d - q axis stator and rotor voltages, while i_{ds} , i_{qs} , i_{dr} , and i_{qr} represent the stator and rotor currents on the same axis. Additionally, ψ_{ds} , ψ_{qs} , ψ_{dr} , and ψ_{qr} indicate the stator and rotor flux components on the d - q axis. The stator and rotor resistances per phase are denoted by R_s and R_r . The stator and rotor inductances are represented by L_s and L_r , respectively, and L_m denotes the magnetizing inductance.

III. SYSTEM MODEL

A. Synchronous Generator Model

The equations governing the two-axis models of the i -th synchronous machine in a multiple-machine network are [26]:

$$\begin{cases} T'_{d0}\dot{E}'_q = -E'_q - \left(\frac{X_d - X'_d}{T'_{d0}} - \frac{T'_{d0} X''_d}{T'_{d0} X'_d} (X_d - X'_d) \right) i_d + E_{fd} \\ T''_{d0}\dot{E}''_q = -E''_q + E'_q - \left(\frac{X'_d - X''_d}{T''_{d0}} + \frac{T''_{d0} X''_d}{T'_{d0} X'_d} (X_d - X'_d) \right) i_d + E_{fd} \\ T'_{q0}\dot{E}'_d = -E'_d - \left(X_q - X'_q - \frac{T'_{q0} X''_q}{T'_{q0} X'_q} (X_q - X'_q) \right) i_q \\ T''_{q0}\dot{E}''_d = -E''_d + E'_d - \left(X_q - X'_q + \frac{T''_{q0} X''_q}{T'_{q0} X'_q} (X_q - X'_q) \right) i_q \\ \dot{\delta} = \Omega_b(\omega - 1) \\ M\dot{\omega} = (P_m - P_e - D(\omega - 1)) \end{cases} \quad (6)$$

The equation includes multiple terms. $E'_{d,q}$ and $E''_{d,q}$ indicate the machine's transient and subtransient voltages along the d - q axis per unit (pu), E_{fd} represents the machine's excitation voltage (pu), $i_{d,q}$ signifies the current on the d - q axis (pu), $X_{d,q}$, $X'_{d,q}$, and $X''_{d,q}$, represent the synchronous, transient, and subtransient reactances along the d - q axis (pu), $T'_{d0,q0}$ and $T''_{d0,q0}$ express the machine's transient and subtransient time constants along the d - q axis (s), δ denotes the machine's rotor angle (rad), Ω_b represents the machine's synchronous base speed (rad/s), ω signifies the machine's rotor speed (pu), M refers to the machine's inertia coefficient (pu.s²/rad), D stands for the machine's damping coefficient (pu.s/rad), P_m indicates the mechanical power applied to the machine shaft (pu), and P_e denotes the electrical power generated by the machine (pu).

B. MBPSS model

The Hydro-Québec-developed MB-PSS [27-28] differs from traditional stabilizers that usually use a series of stacked filters (high-pass and phase-lead-lag). Instead, the MB-PSS consists of three separate stages that work autonomously at low, medium, and high frequencies, making it more robust in different circumstances. The process of selecting the optimum values for Multi-Band Power System Stabilizer (MBPSS) parameters involves a combination of theoretical analysis, simulation studies, and field testing. By utilizing the Genetic Algorithm as an optimization technique, the optimal MBPSS parameters can be ascertained [29]. Based on the simulation studies, the MBPSS parameters are tuned to optimize the controller's performance. The tuning process involves adjusting the gain and time constants of the controller's different bands to achieve the desired damping ratio and bandwidth. The simplified structure comprises three gains K_L , K_I , and K_H ,

which are categorized as low, intermediate, and high, and three frequencies F_L , F_I , and F_H that correspond to low, intermediate, and high frequencies measured in Hz.

IV. RESULTS AND SIMULATION

A. 9-Bus Network

A 9-bus test system was employed for all simulations, as shown in Figure 1. The system consists of three voltage levels, namely 16.5, 18, and 13.8KV, and includes three generators with a 567.5MVA total power output, six transmission lines, and three load nodes with 315MW combined consumption. The generator parameters are specified in the Appendix.

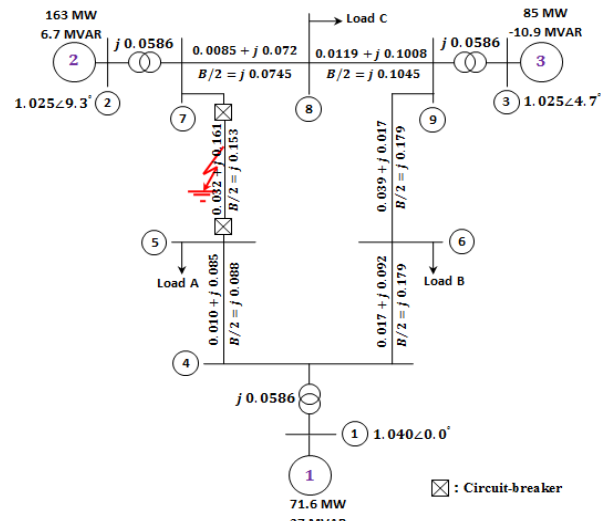


Fig. 1. Nine bus network.

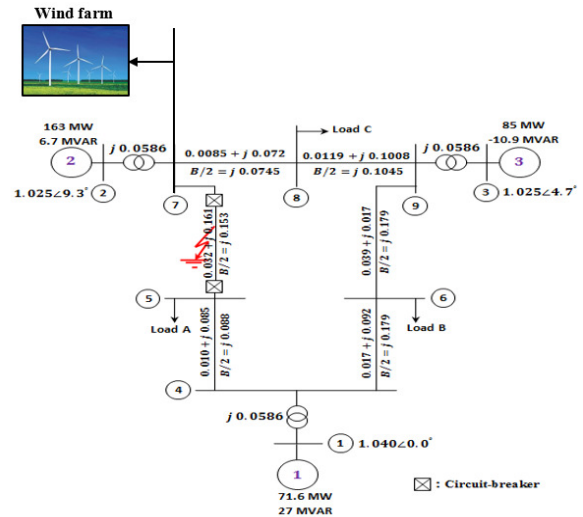


Fig. 2. Nine-bus network with a wind farm.

B. Modified Nine-Bus Network

Multiple strategies can improve the effectiveness of the electrical grid across various stages of the power supply chain, including power generation, transmission, and distribution [30-

32]. Various tests were conducted to determine the optimal wind turbine integration rate and the results showed that bus 7 was the best location for the wind farm. As a result, this location was selected to install a farm consisting of 74 turbines, each generating 1.5MW, for a total capacity of 111MW. The turbine parameters are shown in the Appendix. Figure 2 shows an updated illustration of the grid structure.

C. Applying a Fault in the Proposed System

At time $t=1s$, there was a fault with a duration of 0.1s on the transmission line between nodes 5 and 7. The fault was located in the middle of the line and was classified as an LLLG fault. The modified 9-node WSCC network simulation model was implemented using MATLAB/Simulink. A random wind profile was used to simulate realistic wind conditions, with wind speeds fluctuating between 8 and 14m/s for 10s. Figure 3 shows this time-varying profile which was the basis of the case study.

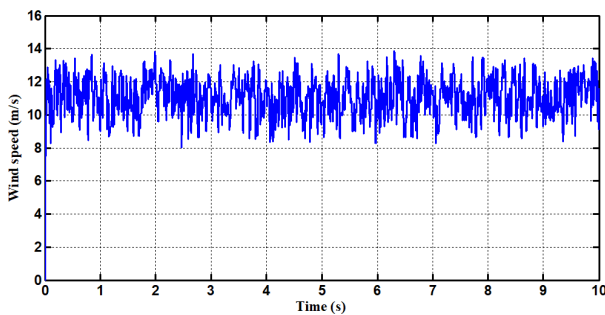


Fig. 3. Wind speed profile.

As mentioned above, the presence of a defect combined with a high level of wind energy integration (35%) results in changes to the power angle and angular speed differences of generators 2 and 3, as well as the frequency at each synchronous generator. To visualize these changes, the Figures below show the evolution of these parameters for two scenarios: (1) without MBPSS, and (2) with MBPSS. The simulation results show that the implementation of MB-PSS in a high wind power integration scenario results in reduced overshoot and faster convergence to the stable equilibrium point, compared to the system without MBPSS. Table I shows a comparison of the damping duration periods for the two scenarios.

TABLE I. DURATION OF DAMPING

Command	Duration of damping
Without MBPSS	>10s
With MBPSS	3s

These data highlight the effectiveness of MBPSS in significantly reducing the damping period of the system. Figures 4 and 5 depict the power angle differences of generators 2 and 3. The power angles δ_{21} and δ_{31} undergo an increase to approximately 58.22° and 33.07° , respectively, followed by subsequent declines to 38.34° and 31.07° for generators 2 and 3. It can be noted that the inclusion of MBPSS results in a reduction of power angle, compared to the system

without it, indicates system stability without any oscillations. The effectiveness of MBPSS in damping oscillations across all frequency ranges is demonstrated in Figures 6 and 7. Specifically, when subjected to an LLLG fault and a 35% wind turbine integration, the system with MBPSS outperforms the one without it. This can be attributed to its multi-stage structure and the presence of three distinct bands, which enable it to efficiently mitigate low-, intermediate-, and high-frequency oscillations.

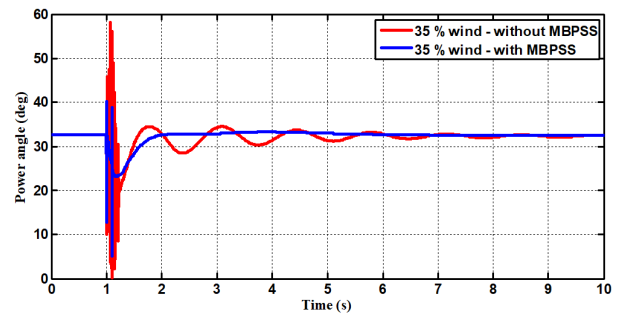


Fig. 4. Power angle variation δ_{21} .

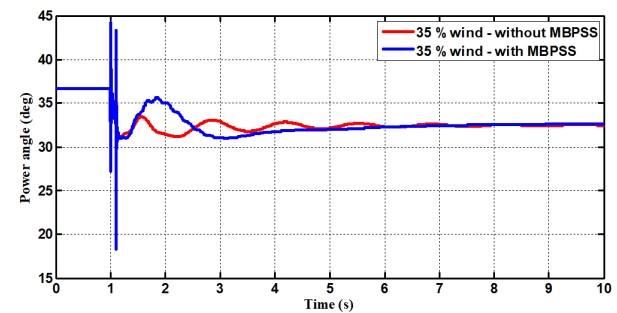


Fig. 5. Power angle variation δ_{31} .

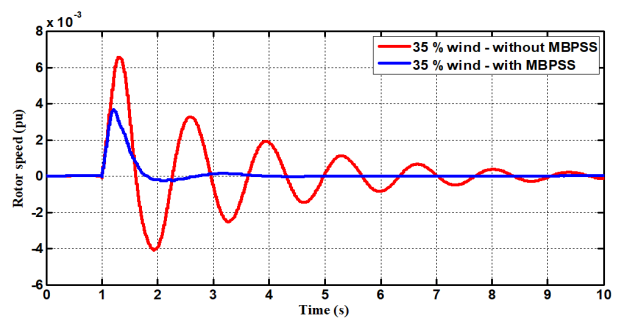


Fig. 6. Angular speed variation ω_{21} .

Figures 8-10 illustrate a significant increase in generator frequencies leading to system instability before the implementation of the MBPSS power regulator. Implementing MB-PSS, the generator frequencies were stabilized and consistently maintained the nominal frequency of 50Hz. Following a severe disturbance (LLLG fault), the simulation results for a 35 % wind turbine integration scenario with the MBPSS regulator indicate a faster response time and shorter stabilization period, compared to the same scenario without it.

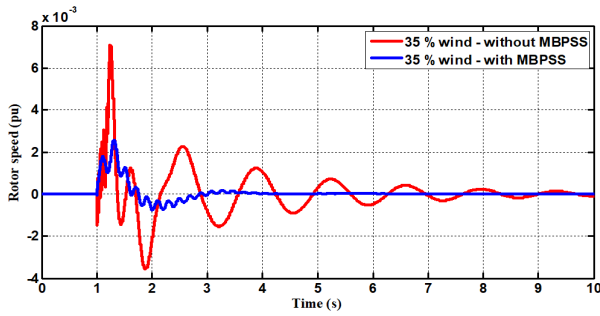


Fig. 7. Angular speed variation ω_{31} .

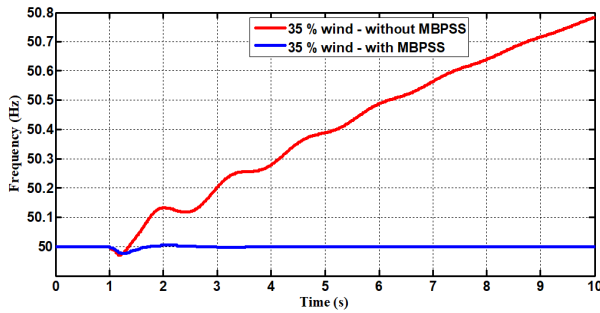


Fig. 8. Frequency profile generator 1.

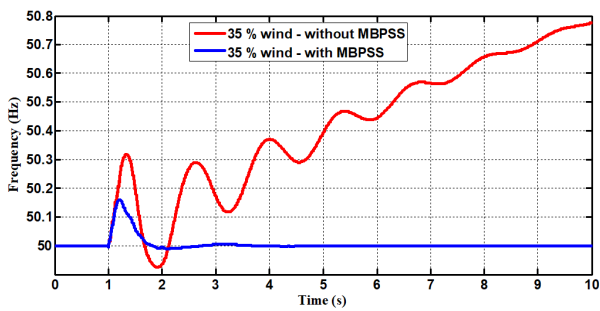


Fig. 9. Frequency profile generator 2.

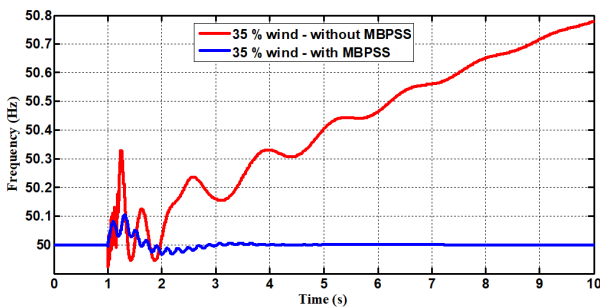


Fig. 10. Frequency profile generator 3.

V. CONCLUSION

This study extensively investigated the modeling and simulation of a high-level wind farm system connected to an electrical network. Dynamic simulations were conducted on a 9-bus multi-machine network that included a wind farm to evaluate the effectiveness and robustness of the MBPSS stabilizer. A wind farm with a capacity of 111MW was installed at bus 7. Using MATLAB/Simulink, this study

analyzed the impact of MBPSS on the transient stability of the power system under failure scenarios, including LLLG faults, and high-level integration of the wind farm. The simulation results indicate a direct correlation between wind farm capacity and power system transient stability. Integrating wind generation at higher levels led to an increase in transient instability. Moreover, the MBPSS was highly effective in enhancing power system stability during high-level integration of wind energy and severe faults and provided adequate damping to all oscillation modes as it consisted of multiple stages with three distinct frequency bands, enabling it to effectively dampen low-, intermediate-, and high-frequency oscillations.

APPENDIX

Table II displays the generator parameters in 'per unit' based on the nominal MVA and KV values. Tables III-V outline the parameters for the wind turbine linked with a DFIG. Tables VI and VII present the MBPSS data for the simplified settings mode and the detailed settings mode, respectively.

TABLE II. GENERATOR PARAMETERS

Generator No:	#1	#2	#3
Rated MVA	247.5	192	128
X_d	0.1460	0.8958	1.3125
X'_d	0.0608	0.1198	0.1813
X''_d	0.0483	0.0891	0.1072
T'_{d0}	8.96	6	5.89
T''_{d0}	0.04	0.033	0.033
X_q	0.0969	0.8645	1.2587
X'_q	0.0969	0.1198	0.1813
X''_q	0.0483	0.0891	0.1072
T'_{q0}	0.31	0.535	0.6
T''_{q0}	0.060	0.08	0.07
R_a	0.0006	0.0013	0.0032
X_l	0.0336	0.0521	0.0742
$H(sec)$	23.64	6.4	3.01

TABLE III. DFIG DATA

Parameters	Value
$S_{nom}(VA)$	1.5e6/0.9
$V_{nom}(V)$	575
$F(Hz)$	50
$R_s(pu)$	0.00706
$Ll_s(pu)$	0.171
$R'_r(pu)$	0.005
$Ll'_r(pu)$	0.156
$L_m(pu)$	2.9
$H(s)$	5.04
p	3

TABLE IV. TURBINE DATA

Parameters	Value
$P_{mec nom}(MW)$	1.5
K_p	500
$\beta(deg)$	50

TABLE V. CONVERTERS DATA

Parameters	Value
P_{max} (pu)	0.5
[L R] (pu)	[0.15 0.0015]
[IL (pu) ph_{IL} (deg)]	[0 90]
V_{dc} (V)	1200
C (F)	10000e-6

TABLE VI. MBPSS DATA FOR SIMPLIFIED SETTINGS MODE

Parameters	Value
Low frequency band: [F_L (Hz) K_L]	[0.2 20]
Intermediate frequency band: [F_I (Hz) K_I]	[0.9 25]
High frequency band: [F_H (Hz) K_H]	[12 145]
Signal limits [V_{lmax} V_{lmax} V_{Hmax} V_{Smax}]	[0.75 0.15 0.15 0.15]

TABLE VII. MBPSS DATA FOR DETAILED SETTINGS MODE

Parameters	Value
Low frequency gains: [K_{L1} K_{L2} K_L]	[66 66 9.4]
Low frequency time constants: [T_{L1} T_{L2} T_{L3} T_{L4} T_{L5} T_{L6} T_{L7} T_{L8} T_{L9} T_{L10} T_{L11} T_{L12} K_{L11} K_{L17}]	[1.667 2 0 0 0 0 2 2.4 0 0 0 1 1]
Intermediate frequency gains: [K_{I1} K_{I2} K_I]	[66 66 47.6]
Low frequency time constants: [T_{I1} T_{I2} T_{I3} T_{I4} T_{I5} T_{I6} T_{I7} T_{I8} T_{I9} T_{I10} T_{I11} T_{I12} K_{I11} K_{I17}]	[1 1 0.25 0.3 0 0 1 1 0.3 0.36 0 0 0 0]
Intermediate frequency gains: [K_{H1} K_{H2} K_H]	[66 66 233]
Low frequency time constants: [T_{H1} T_{H2} T_{H3} T_{H4} T_{H5} T_{H6} T_{H7} T_{H8} T_{H9} T_{H10} T_{H11} T_{H12} K_{H11} K_{H17}]	[0.01 0.012 0 0 0 0 0.012 0.0144 0 0 0 1 1]

REFERENCES

[1] Y. Wang *et al.*, "Where is the most feasible, economical, and green wind energy? Evidence from high-resolution potential mapping in China," *Journal of Cleaner Production*, vol. 376, Nov. 2022, Art. no. 134287, <https://doi.org/10.1016/j.jclepro.2022.134287>.

[2] G. M. Shafiqullah, A. M.T. Oo, A. B. M. Shawkat Ali, and P. Wolfs, "Potential challenges of integrating large-scale wind energy into the power grid—A review," *Renewable and Sustainable Energy Reviews*, vol. 20, pp. 306–321, Apr. 2013, <https://doi.org/10.1016/j.rser.2012.11.057>.

[3] S. H. Qazi and M. W. B. Mustafa, "Technical Issues on Integration of Wind Farms with Power Grid- A Review," *International Journal of Sustainable and Green Energy*, vol. 3, no. 5, Sep. 2014, Art. no. 87, <https://doi.org/10.11648/j.ijrse.20140305.11>.

[4] T. G. Tran, T. A. Nguyen, M. V. N. Hoang, N. A. Nguyen, and T. T. Tran, "Load Shedding in High-Integrated Wind Energy Power Systems Using Voltage Electrical Distance," *Engineering, Technology & Applied Science Research*, vol. 12, no. 2, pp. 8402–8409, Apr. 2022, <https://doi.org/10.48084/etasr.4779>.

[5] R. Terzioğlu and T. Fedai, "Probabilistic Load Flow Analysis of the 9 Bus WSCC System," *International Journal of Scientific and Research Publications*, vol. 3, no. 9, Sep. 2013.

[6] R. Kaur and D. Kumar, "Transient Stability Improvement of IEEE 9 Bus System Using Power World Simulator," *MATEC Web of Conferences*, vol. 57, 2016, Art. no. 01026, <https://doi.org/10.1051/mateconf/20165701026>.

[7] B. Ramlochun, C. A. Vaithilingam, A. A. Alsakati, and J. Alnasseir, "Transient stability analysis of IEEE 9-bus system integrated with DFIG and SCIG based wind turbines," *Journal of Physics: Conference Series*, vol. 2120, no. 1, Sep. 2021, Art. no. 012023, <https://doi.org/10.1088/1742-6596/2120/1/012023>.

[8] A. A. Alsakati, C. A. Vaithilingam, and J. Alnasseir, "Transient Stability Assessment of IEEE 9-Bus System Integrated Wind Farm," *MATEC Web of Conferences*, vol. 335, 2021, Art. no. 02006, <https://doi.org/10.1051/mateconf/202133502006>.

[9] M. Farahani, "Damping of subsynchronous oscillations in power system using static synchronous series compensator," *IET Generation, Transmission & Distribution*, vol. 6, no. 6, pp. 539–544, Jun. 2012, <https://doi.org/10.1049/iet-gtd.2011.0625>.

[10] B. Tang, M. L. McAnelly, and G. Gu, "Experimental parameter tuning of power system stabilizer," in *2012 24th Chinese Control and Decision Conference (CCDC)*, Taiyuan, China, Feb. 2012, pp. 2132–2137, <https://doi.org/10.1109/CCDC.2012.6244341>.

[11] M. O. Hassan, S. J. Cheng, and Z. A. Zakaria, "Design and parameters optimization of power system stabilizer to improve power system oscillations," in *2010 The 2nd International Conference on Computer and Automation Engineering (ICCAE)*, Singapore, Oct. 2010, vol. 5, pp. 107–111, <https://doi.org/10.1109/ICCAE.2010.5451504>.

[12] A. J. Urdaneta, N. J. Bacalao, B. Feijoo, L. Flores, and R. Diaz, "Tuning of power system stabilizers using optimization techniques," *IEEE Transactions on Power Systems*, vol. 6, no. 1, pp. 127–134, Oct. 1991, <https://doi.org/10.1109/59.131055>.

[13] Y. Zhang, G. P. Chen, O. P. Malik, and G. S. Hope, "An artificial neural network based adaptive power system stabilizer," *IEEE Transactions on Energy Conversion*, vol. 8, no. 1, pp. 71–77, Mar. 1993, <https://doi.org/10.1109/60.207408>.

[14] M. Klein, L. X. Le, G. J. Rogers, S. Farrokhpay, and N. J. Balu, "H/sub spl infin damping controller design in large power systems," *IEEE Transactions on Power Systems*, vol. 10, no. 1, pp. 158–166, Oct. 1995, <https://doi.org/10.1109/59.373938>.

[15] H. J. C. Peiris, U. D. Annakkage, and N. C. Pahalawaththa, "Generation of fuzzy rules to develop fuzzy logic modulation controllers for damping of power system oscillations," *IEEE Transactions on Power Systems*, vol. 14, no. 4, pp. 1440–1445, Aug. 1999, <https://doi.org/10.1109/59.801922>.

[16] R. Grondin, I. Kamwa, G. Trudel, L. Gerin-Lajoie, and J. Taborda, "Modeling and closed-loop validation of a new PSS concept, the multi-band PSS," in *2003 IEEE Power Engineering Society General Meeting (IEEE Cat. No.03CH37491)*, Toronto, ON, Canada, Jul. 2003, vol. 3, pp. 1804–1809, <https://doi.org/10.1109/PES.2003.1267430>.

[17] R. Grondin *et al.*, "The multi-band PSS, a flexible technology designed to meet opening markets," in *Proceedings CIGRE 2000*, 2000.

[18] D. Rimorov, A. Heniche, I. Kamwa, G. Stefopoulos, S. Babaei, and B. Fardanesh, "Inter-area oscillation damping and primary frequency control of the New York state power grid with multi-functional multi-band power system stabilizers," in *2016 IEEE Power and Energy Society General Meeting (PESGM)*, Boston, MA, USA, Jul. 2016, pp. 1–5, <https://doi.org/10.1109/PESGM.2016.7943312>.

[19] D. Rimorov, A. Heniche, I. Kamwa, S. Babaei, G. Stefopoulos, and B. Fardanesh, "Dynamic performance improvement of New York state power grid with multi-functional multi-band power system stabiliser-based wide-area control," *IET Generation, Transmission & Distribution*, vol. 11, no. 18, pp. 4537–4545, 2017, <https://doi.org/10.1049/iet-gtd.2017.0288>.

[20] M. Alrifai, M. Zribi, and M. Rayan, "Feedback Linearization Controller for a Wind Energy Power System," *Energies*, vol. 9, no. 10, Oct. 2016, Art. no. 771, <https://doi.org/10.3390/en9100771>.

[21] M. A. Zdiri, B. Dhoubi, Z. Alaas, and H. Hadj Abdallah, "A Low-Voltage AC, Low-Voltage DC, and High-Voltage DC Power Distribution System with Grid: Design and Analysis," *Applied Sciences*, vol. 13, no. 2, Jan. 2023, Art. no. 808, <https://doi.org/10.3390/app13020808>.

[22] D. Aguglia, P. Viarouge, R. Wamkeue, and J. Cros, "Determination of fault operation dynamical constraints for the design of wind turbine DFIG drives," *Mathematics and Computers in Simulation*, vol. 81, no. 2, pp. 252–262, Oct. 2010, <https://doi.org/10.1016/j.matcom.2010.05.001>.

[23] B. Dhoubi, Z. Alaas, O. Kahouli, and H. Haj Abdallah, "Determination of optimal location of FACTS device to improve integration rate of wind energy in presence of MBPSS regulator," *IET Renewable Power Generation*, vol. 14, no. 17, pp. 3526–3540, 2020, <https://doi.org/10.1049/iet-rpg.2020.0679>.

[24] A. Guediri and S. Touil, "Modeling and Comparison of Fuzzy-PI and Genetic Control Algorithms for Active and Reactive Power Flow between the Stator (DFIG) and the Grid," *Engineering, Technology &*

- Applied Science Research*, vol. 12, no. 3, pp. 8640–8645, Jun. 2022, <https://doi.org/10.48084/etasr.4905>.
- [25] L. N. Widanagama Arachchige, A. D. Rajapakse, and D. Muthumuni, "Implementation, Comparison and Application of an Average Simulation Model of a Wind Turbine Driven Doubly Fed Induction Generator," *Energies*, vol. 10, no. 11, Nov. 2017, Art. no. 1726, <https://doi.org/10.3390/en10111726>.
- [26] J. Machowski, Z. Lubosny, J. W. Bialek, and J. R. Bumby, *Power System Dynamics: Stability and Control*. Hoboken, NJ, USA: John Wiley & Sons, 2020.
- [27] P. He, F. Wen, G. Ledwich, Y. Xue, and K. Wang, "Effects of various power system stabilizers on improving power system dynamic performance," *International Journal of Electrical Power & Energy Systems*, vol. 46, pp. 175–183, Mar. 2013, <https://doi.org/10.1016/j.ijepes.2012.10.026>.
- [28] A. Khodabakhshian, R. Hemmati, and M. Moazzami, "Multi-band power system stabilizer design by using CPCE algorithm for multi-machine power system," *Electric Power Systems Research*, vol. 101, pp. 36–48, Aug. 2013, <https://doi.org/10.1016/j.epsr.2013.03.011>.
- [29] B. Dhoubi, Z. Alaas, A. Kahouli, and H. H. Abdallah, "Parameters Optimization of AVR and Multi-Band PSS via Genetic Algorithm Technique so as to Improve the Integration Rate of Wind Farm into the Electricity Grid," *PONTE International Journal of Science and Research*, vol. 75, no. 12, Dec. 2019, <https://doi.org/10.21506/j.ponte.2019.12.9>.
- [30] B. K. Ponukumati, P. Sinha, M. K. Maharana, A. V. P. Kumar, and A. Karthik, "An Intelligent Fault Detection and Classification Scheme for Distribution Lines Using Machine Learning," *Engineering, Technology & Applied Science Research*, vol. 12, no. 4, pp. 8972–8977, Aug. 2022, <https://doi.org/10.48084/etasr.5107>.
- [31] T. Le and B. L. N. Phung, "Load Shedding in Microgrids with Consideration of Voltage Quality Improvement," *Engineering, Technology & Applied Science Research*, vol. 11, no. 1, pp. 6680–6686, Feb. 2021, <https://doi.org/10.48084/etasr.3931>.
- [32] M. A. Zdiri, B. Dhoubi, Z. Alaas, F. B. Salem, and H. H. Abdallah, "Load Flow Analysis and the Impact of a Solar PV Generator in a Radial Distribution Network," *Engineering, Technology & Applied Science Research*, vol. 13, no. 1, pp. 10078–10085, Feb. 2023, <https://doi.org/10.48084/etasr.5496>.